This document is downloaded from DR-NTU (https://dr.ntu.edu.sg)
Nanyang Technological University, Singapore.

Asymmetric electron transport realized by decoupling between molecule and electrode

Liu, Hongmei; Zhao, Jianwei; Boey, Freddy Yin Chiang; Zhang, Hua

2009

Liu, H., Zhao, J., Boey, F. Y. C., & Zhang, H. (2009). Asymmetric electron transport realized by decoupling between molecule and electrode. Physical Chemistry Chemical Physics, 11(44), 10323-10330.

https://hdl.handle.net/10356/95130

https://doi.org/10.1039/b914090e

© 2009 the Author(s). This is the author created version of a work that has been peer reviewed and accepted for publication by Physical Chemistry Chemical Physics, the Owner Societies. It incorporates referee’s comments but changes resulting from the publishing process, such as copyediting, structural formatting, may not be reflected in this document. The published version is available at: [doi:http://dx.doi.org/10.1039/b914090e].

Downloaded on 02 Dec 2023 20:18:36 SGT

Asymmetric electron transport realized by decoupling between molecule and electrode†

Hongmei Liu[a], *Jianwei Zhao**[a], *Freddy Boey*[b], *and Hua Zhang*[b]

[a]*Key Laboratory of Analytical Chemistry for Life Science (Ministry of Education), School of Chemistry and Chemical Engineering, Nanjing University, Nanjing 210008, P. R. China.*
E-mail: zhaojw@nju.edu.cn

[b]*School of Materials Science and Engineering, Nanyang Technological University, 50 Nanyang Avenue, Singapore 639798, Singapore*

†*Electronic supplementary information (ESI) available: The electron transport of linear models with different molecular proportion and the charge distribution calculated by different methods.*

Abstract

We studied the contact coupling effect on the asymmetric electron transport in molecular junctions by the first-principles density functional theory incorporating with the non-equilibrium Green's function method. To realize the decoupling, a rigid saturated ring is inserted into the metallic electrode and conjugated molecular bridge (linear oligo phenylene ethynylene and cyclic porphine). As a tunneling barrier, the saturated ring reduces the conductance by 2–3 orders of magnitude. However, the electronic decoupling greatly improves the asymmetric electron transport. In the case of the linear system, the favorite direction of electron transport is from the strong coupling end to the weak coupling one with a rectification ratio of 5 at 2.0 V.
In addition, the rectification performance is sensitive to the molecular proportion of the molecular wire length and the tunneling barrier width. When the same barrier is applied, shortening the length of conjugated part can reduce rectification performance. The mechanism of rectification is analyzed by means of the potential drop, the spatial distribution of the molecular orbitals and the transmission spectra.

1. Introduction

Since Aviram and Ratner[1] proposed that an organic molecule could function as a molecular diode, the idea of using organic molecules as functional units in electronic devices has received great attention. In recent decades, tremendous theoretical and experimental efforts were focused on the Aviram–Ratner (A–R) type of molecular rectifier.[2–5] One way to construct A–R rectifiers is to introduce asymmetric side substitutions on the electron transport pathway, in which the electron-donating and withdrawing groups serve as the *n*-doping and *p*-doping, respectively.[6] However, due to the strong coupling *via* the p-linkage, the side-substitution is hard to provide high rectification performance.[6,7] Many theoretical investigations6,8 and experimental measurement results[9–11] also demonstrated that the asymmetric junction cannot always cause the rectification. Therefore, the remaining challenge is to clarify when the rectification can appear for the asymmetric molecular junction and how significant the rectification is.

In the molecular devices, many factors affect the electron transport: namely, the electrode material,[10] interface,[12–14] anchoring groups,[15–17] end connecting position,[18–20] molecular bridge,[10,21,22] electron transport pathway,[23,24] and environment.[8,25,26] Among them, the electronic coupling between the conjugated molecular wire and metallic electrode also plays an important role in the electron transport. Therefore, controlling the interfacial electronic coupling is an effective approach to the molecular rectification. By changing the electrode geometry and contact area, Basch *et al.*[27] modulated the interfacial coupling and found that variations in molecular conductance are of the order 0–300%. Using different anchoring groups, [28] asymmetric contact was established and the studies of electron transport evidenced the rectification of the molecular junction. Recently, Taylor *et al.*[29] theoretically demonstrated that the asymmetric molecule– electrode coupling, *i.e.* chemisorption at one end of the junction and physisorption at the other, can improve the rectification performance of the molecular junction.

Although the physical contact can much reduce the coupling between the conjugated molecular bridge and the metal electrode, it cannot provide a perfect alignment of molecular level to the electrode Fermi level. This may result in other electron transport mechanisms involved in the molecular junction. To overcome this drawback, in this paper we propose to use a controllable tunneling barrier that can be covalently bonded to the molecular bridge and the electrode. This configuration allows a better coupling at the interface, but also induces decoupling at one molecular end. We used first-principles density functional theory (DFT) and the non-equilibrium Green's function (NEGF) formalism[30] to study the effect of tunneling barrier in the linear and cyclic molecules coupled to the metallic electrodes. The molecular structures of all models are shown in Scheme 1. The linear molecules are oligo (phenylene ethynylene) (OPE), [31] forming a long rigid molecule with π-conjugated and delocalized frontier orbitals. The cyclic system consisting of porphine has a low molecular proportion. Here, we defined the molecular proportion (R) as the ratio of the length of the conjugated wire (L_c) to the saturated ring (L_s), *i.e.* $R = L_c/L_s$, which is 6.4 and 2.9 for the linear and cyclic systems, respectively. The rectification was realized by tuning the degree of the molecule–electrode decoupling and the molecular proportion.

2. Methodology

In order to reveal the influence of the barrier to the electron transport, we investigated two systems, *i.e.* the linear and cyclic systems with different molecular proportion. For all the models, the thiol groups at two ends of the molecules are bonded to the Au electrodes, which provide efficient electronic coupling at interfaces. In the case of linear system, the first model is symmetric OPE. While in the second model OPE–Oc, one end of the molecule is terminated by saturated bridge (bicyclo[2.2.2]octane). For the cyclic systems, we compared three types of connections to the electrode. The first model is porphine (Por) with symmetric contact. The second is benzene connected porphine (Por–Ph) with a twisting angle, in which the electronic coupling is reduced by the twisted benzene ring. The third is bicyclo[2.2.2]octane connected porphine (Por–Oc), in which the a-bridge at one side greatly reduces the coupling.

The DFT and NEGF approach is utilized to describe the behavior of molecular junctions under nonequilibrium conditions. We used the Atomistix Toolkit[32] program to simulate the electron transport properties of two-probe systems. A molecule is embedded in a unit cell of Au(111) surfaces. In the model for the electron transport calculation, the molecular junction is divided into three regions: left electrode, scattering region, and right electrode. The semi-infinite electrodes are calculated separately to obtain the bulk self-energy. The scattering region contains parts of the electrodes to include the screening effects in the calculations, 18 Au atoms of the left (two 3 x 3 layers of Au surfaces) and 27 of the right electrode (three 3 x 3 layers of Au surfaces). This is the unit cell, where the difference in the number of atoms of electrode is necessary to maintain the periodicity of the system.[33]

The geometries of the molecules were firstly optimized at the B3LYP/6-31G* theoretical level by the Gaussian 03 software,[34] as described in detail in our previous papers.[7,23,24] Then, the model molecules lost hydrogen atoms and were perpendicular to the Au surface. The sulfur atoms were placed above a threefold hollow site of the Au plane at a distance of 2.0 Å.[35] All the atoms in the molecules were relaxed while the electrodes were fixed at their bulk positions until the force on each atom was less than 0.05 eV $Å^{-1}$. We used a double-ζ plus the polarization basis set for the organic molecules, and a single-ζ plus the polarization basis set for the gold electrodes with local density approximation (LDA). After the geometric optimization by Atomistix Toolkit,[32] a bias was applied between the two electrodes and the current was generated using the NEGF formalism.

3. Results and discussion

3.1 The decoupling effect in the linear system

The spatial distribution of frontier orbital is a static feature of the molecule, which describes the mobility of the π-electron in the conjugated molecule. It is a three-dimensional representation of the local density of states and visually gives the electron density of the molecules. Fig. 1 shows the HOMO (the highest occupied molecular orbital) and LUMO (the lowest unoccupied molecular orbital) of linear system as well as the projected density of states (PDOS) at zero bias. The left panel of Fig. 1a plots the PDOS of OPE. Two peaks are observed at 0.5 eV below and 1.6 eV above Fermi level $E_F = 0$, originating from the HOMO and the LUMO, respectively.

From the right panel, we can observe that both the HOMO and the LUMO are fully delocalized across the OPE molecule. In contrast, for the OPE–Oc shown in Fig. 1b, high orbital density on the left sulfur atom allows a better coupling of the molecule to the left electrode. However, the saturated bridge blocks the coupling between molecule and right electrode. The decoupling of molecule may impose an internal barrier to electron transport through the molecule, which will significantly affect the transport behavior. Additionally, from the PDOS in Fig. 1b, the saturated ring of OPE–Oc not only sharpens the intensity of the HOMO resonance wave but also shifts down the HOMO resonance in energy (by 0.5 eV) compared with OPE. Therefore, a sharp peak in PDOS at -1.0 eV corresponds to the localized HOMO of OPE–Oc.

Based on the qualitative analysis of the spatial distribution, we further performed the natural bond orbital (NBO) analysis of OPE–Oc at the B3LYP level of theory (with 6-31G* basis set for molecule and LanL2DZ basis set for Au). Fig. 2a shows the potential drop of the OPE–Oc embedded in Au electrodes at 1.5 V. Since the conjugated π-segment of OPE–Oc is linked to the left electrode and the saturated ring to the right side, the potential drop is highly non-uniform due to the different degree of electronic coupling. A covalent σ-segment is much more localized than a conjugated π-segment as mentioned above. Therefore, the conjugated OPE part reduces the potential whereas the saturated ring slightly modifies the potential. The potential along the saturated ring drops rapidly than that along the conjugated molecular backbone. A nonlinear potential drop induced by an intrinsic asymmetry in the molecule may cause rectification.

To analyze the potential drop across the molecular junction, we gave the relative electric charge (with respect to zero bias) of isolated OPE–Oc and Au–OPE–Oc–Au. We divided the molecule OPE–Oc into 8 parts by dotted lines as shown in Fig. 2a. From the relative electric charge in Fig. 2b and c, it can be seen that the conjugated phenyl rings are easily polarized by the external electric field, especially part 6 (the phenyl ring near the saturated ring). The relative charge of part 6 at 1.5 V reaches 0.010 and 0.015 e for isolated OPE–Oc and Au–OPE–Oc–Au, respectively. In contrast to the conjugated part, the electric charge of the saturated ring only changes slightly, regardless of the electrodes, which is consistent with the non-uniform potential drop. In addition, the B3LYP method suffers from the self-interaction and usually overestimates the molecular polarizability.[36,37] To correct this error, Baer *et al.* developed approaches to DFT with correct long-range behavior.[38,39] In order to evaluate the effect of the self-interaction on the present system, we have performed the charge distribution analysis for the OPE–Oc by other methods, *i.e.* the B3PW91, X3LYP and HF methods (see ESI). In spite of various methods used, the relative charge distribution along the molecular axis is essentially identical. Therefore, we can conclude that the results obtained by B3LYP for these systems are reliable.

Now, we focus on the decoupling effect directly by comparison of the current–voltage (*I–V*) curves as shown in Fig. 3a for the linear system. It is clearly seen that the OPE conducts better than OPE–Oc. Since strong electronic coupling at two ends is generally expected to give larger delocalization of the π orbitals on the molecules. The conductance of OPE at zero bias is 3.4 μS, which is near 3 orders of magnitude greater than that of OPE–Oc (0.005 μS). Furthermore, the *I–V* curve of OPE is symmetric due to the molecular structure and molecule–electrode interface. However, in the case of model OPE–Oc (the inset of Fig. 3a), the negative current increases more dramatically than the positive one as the bias is over 1.2 V. Then the OPE–Oc shows pronounced rectification behavior. Although there is no any asymmetric substitution, obvious asymmetric electron transport behavior has been observed in the

specific system.

To clearly explore the asymmetric electron transport of OPE–Oc induced by the tunneling barrier, we plotted the rectification ratio as a function of the applied bias (Fig. 3b), where the rectification ratio (RR) is defined as the absolute current value at negative bias over that at corresponding positive bias, i.e. $RR = \frac{|I(-V)|}{|I(+V)|}$. The model OPE–Oc exhibits pronounced rectification ratio of 5 at 2.0 V. As a result, the electron flow is favored from the left side to the right side. In other words, the favorite direction is from the high coupling side to the weak coupling side, which is consistent with the demonstration of Taylor *et al.*[29] The result reveals that the inserted barrier in molecule can induce asymmetric electron transport. This decoupling effect in the present study is quite different from the physical binding to electrodes at one end of molecule in previous study.[29] The insertion of a tunneling barrier in molecule not only allows chemical bonding to the electrodes via thiol groups, but also leads to rectification.

As an original description of the asymmetric electron transport, the calculated transmission spectra $T(E,V_b)$ as a function of electron energy are plotted in Fig. 4a and b. The current is obtained by the Landauer–Büttiker formula $I = \int T(E,V_b)dE$. The energy region which contributed to the current integral above, which we refer to as the *bias window*, is indicated as the gray region. The first transmission peak below the Fermi level $E_f = 0$ is the HOMO resonance, while the LUMO resonance is the first peak above $E_f = 0$. For OPE in Fig. 4a, we find that the metal Fermi level situates closer to the HOMO than the LUMO (LUMO located above 1.5 eV). The stronger the molecule–electrode coupling, the larger the mixing between the discrete molecular levels with the continuum metal electronic states. Strong coupling between the Au electrode and two ends of OPE leads to a broad transmission spectrum around the Fermi level.[40] Therefore, a large conductance at zero bias is originated from the resonant tunneling of HOMO.

From the logarithmic plot of transmission for OPE–Oc in Fig. 4b, it can be observed that the HOMO and LUMO resonance are all very weak, corresponding to $T \sim 10^{-2}$. Smaller tunneling channels open when the molecule–electrode coupling at one end is broken by the saturated bridge. Due to the tunneling barrier and weak transmission resonance, the conductance of OPE–Oc is much lower than that of OPE. In addition, all the LUMO resonances are out of the bias window (gray region) under both positive and negative bias. The negative bias (-2.0 V), which drives the HOMO resonance, enters the bias window and the transmission coefficient at $E_f = 0$ is then about 5×10^{-3}. However, the HOMO resonance under positive bias is out of the energy region and transmission coefficient at Fermi level is less than 10^{-4}. Therefore the negative current is larger than the positive one, resulting in obvious rectification.

Another feature of the junction is the molecular projected self-consistent Hamiltonian (MPSH),[41] which is the self-consistent Hamiltonian of the isolated molecule in the presence of Au electrode, namely, the molecular part extracted from the whole self-consistent Hamiltonian for the scattering region. Fig. 4c and d plot the dependence of molecular orbital energy levels upon applied bias for models OPE and OPE–Oc. The shadow regions denote the bias window in the transmission spectra. From Fig. 4c, we can observe that the HOMO energy level of OPE slightly increases with bias. Since the symmetric molecule–electrode coupling, the HOMO shows symmetric evolution at two sides and enters the bias window at 1.2 V. However, in Fig. 4d, the HOMO energy level of OPE–Oc asymmetrically responds to the bias, which is out of the bias window during the positive region and enters the bias window at -1.0 V. Therefore, the HOMO contributes to the current and is responsible for the

asymmetric current of OPE–Oc.

To summarize, the saturated ring efficiently blocks the electronic coupling in the linear system and serves as a tunneling barrier. The insertion of a tunneling barrier at one end of the linear molecule could induce asymmetric electron transport. Now, one question raised here is whether the barrier width affects the asymmetric electron transport? Note that the molecular proportion of OPE–Oc is 6.4. Therefore, we also studied other linear models with conjugated parts of shorter lengths (R = 1.1 and 3.7), for which almost symmetric *I–V* curves are observed (see ESI). To further gain insight into the influence of molecular proportion, we discussed the cyclic system as follows.

3.2 The decoupling effect in the cyclic system

Comparing with the linear conjugated molecules, the cyclic porphine has more electron transport pathways[23] and is highly conductive due to the macro-π conjugation.[42] The conductance at zero bias of porphine (73.8 μS) is 20 times that of OPE (3.4 μS). Importantly, the porphine has a lower band gap of 1.74 eV and short length of 7.61 Å, forming an instructive model of Por–Oc with a molecular proportion R = 2.9. Fig. 5a shows the *I–V* curves of the porphine system and the inset is the *I–V* curve of Por–Oc. For the models of Por and Por–Ph with zero bias conductance of 73.8 and 44.5 μS, respectively, a good electronic coupling is established by the fully-conjugated cyclic unit. Comparing with the pure porphine molecule,[43] the introduction of the phenyl ring almost does not affect the conductance, though the electron scattering distance increases from 10.9 Å (Por) to 15.0 Å (Por–Ph). This result also indicates a strong coupling between porphine and phenyl group. However, the existence of the saturated bridge can impede the communication between the π-electrons of the conjugated unit and the *d*-band of the metallic electrode. Due to this decoupling, the conductance at zero bias of Por–Oc (0.17 μS) is two orders of magnitude lower than that of the Por molecule.

Fig. 5b shows the rectification ratio as a function of the applied bias. Obviously, the model Por does not show rectification, because it is symmetric and well-coupled to the electrodes. From the geometric observation, the model Por–Ph is found to be distorted due to the steric hindrance, therefore, the intramolecular coupling is not as good as that in the model Por. Consequently, only slight rectification ratio is observed. Similar behavior is found for the model Por–Oc as one-side coupling between molecule and electrode is broken. As the bias is 0.4 V, molecular rectification can be observed for the Por–Oc molecule and the maximum rectification ratio reaches 1.7. However, the rectification direction reverses at 1.4 V for Por–Oc. Therefore, we can conclude that the small molecular proportion reduces the rectification. The slight rectification of Por–Oc is consistent with the linear models with R = 1.1 and 3.7 given in the ESI.

To provide insight into the effect of molecular porportion, we further analyzed the transmission spectra of the three models, as shown in Fig. 6. Due to the well-coupled structure of Por, the energy level of HOMO in the model Por is very close to the Fermi level (Fig. 6a), so that the HOMO resonance becomes the main contributor to the current. In the logarithmic plot of transmission of Por–Oc at zero bias (Fig. 6c), the HOMO located at -0.5 eV forms a broad resonance. When a small bias is applied, the bias window is too narrow to include the main transmission wave contributed by the LUMO resonance, but it may cover the part of HOMO transmission wave. Under this condition, the variations of both energy level transmission intensity are not significant to the asymmetric electron transport. As a result, slight rectification is

observed at low bias. However, when the bias is above 1.4 V, the strong electric field drives either HOMO or LUMO or both of them to shift into the bias window, and can even greatly enhance the transmission probability at the positive bias. Consequently, the current at positive bias is larger than that at the corresponding negative bias, changing the rectification direction. In contrast to OPE–Oc, the small molecular proportion promotes the contribution of LUMO to the bias window at larger positive bias. As a result, the rectification direction reverses. Similar feature is also found in the model Por–Ph (Fig. 6b). In addition, the coupling also leads to the pinning of the HOMO position in Por–Ph, in spite of the applied bias. Obviously, this pinning effect makes the molecule lose its rectification ability.

In fact the energy level of molecular orbitals also changes with the applied bias which makes the system deviates from the equilibrium state. To describe the energy levels of molecule itself, we analyzed the MPSH of molecular orbitals. Fig. 6d–f show the relation between molecular orbital energy levels and bias. In the case of Por shown in Fig. 6d, when bias is applied, the orbital energy levels of Por are symmetric under positive and negative bias. Within the researched bias range (-2.0 V to 2.0 V), only the HOMO enters the bias window at 1.0 V. However, the orbital energy levels of Por–Ph and Por–Oc shift asymmetrically under positive and negative bias.

The shift trends of LUMO and LUMO + 1 are very similar. For Por–Ph in Fig. 6e, the HOMO enters into the bias window at 0.6 V under negative voltage. With increasing bias, the HOMO and LUMO of Por–Ph molecule also enter into the bias window at 1.2 and 1.6 V, respectively, under positive bias. This is responsible for the reverse of the rectification direction. A similar trend could be found in Fig. 6f: the HOMO of Por–Oc enters into the bias window at 0.6 V under negative bias, resulting in the weak rectification ratio of 1.7. As the bias increases, LUMO and LUMO + 1 of the Por–Oc molecule also enter into the bias window at 1.4 V, which gives rise to a reversal of the rectification direction.

From the electron transport behavior, we can conclude that although there is no asymmetric substitution to the conjugated backbone, the molecular rectification is evidenced. However, the rectification also depends on the molecular proportion *R*. The small *R* not only reduces the rectification ratio, but also reverses the rectification direction at large bias. This behaviour is impossible to interpret using classical tunnelling theory.[44] In the classical framework, the molecular bridge serves as the tunneling barrier. Despite of the shape of the barrier, the integral current should be symmetric, if the barrier meets the requirement of the WKB (Wentzel–Kramers–Brillouin) approximation. To elucidate the molecular rectification in these systems, we plotted the PDOS and the spatial distribution of the frontier molecular orbital of the cyclic system (Fig. 7). In general, porphine makes a major contribution to bothHOMO and LUMO in all models. From Fig. 7a, it is clearly observed that the molecule Por is fully conjugated. For model Por–Ph (left panel in Fig. 7b), the conjugated part of phenyl group also contributes to the frontier molecular orbitals, and partial disconnection of the π-conjugation is caused from the distortion between two rings. This character becomes more obvious when the coupling at one side is completely broken as presented by the model Por–Oc. Because of its saturated nature (right panel in Fig. 7b), a remarkably localized HOMO and LUMO are observed for the Por–Oc molecule. Importantly, the HOMO only forms a weak resonance in PDOS for all the cyclic models. This characteristic is quite different from the linear OPE–Oc, in which the inserted ring leads to a sharp HOMO resonance peak. In other words, because of the low molecular proportion of Por–Oc, the inserted saturated ring only

slightly modifies the intensity of HOMO resonance and the position of HOMO energy level. The static features also confirm the weakly asymmetric electron transport. The intuitive presentation of the orbital spatial distribution given in Fig. 7 is in good agreement with the quantitative result of the transmission spectrum.

Further evidence for the characteristic of Por–Oc is provided by Fig. 8, which shows the potential drop along the Por–Oc junction and the electric charge of the Por–Oc under the external electric field. The non-uniform potential drop is similar with OPE–Oc junction. The conjugated porphine ring greatly slows the gradient of potential drop, whereas the saturated ring slightly affects the potential. We also divided the molecule Por–Oc into 4 parts by dotted lines. From the relative electric charge of Por–Oc and Au–Por–Oc–Au in Fig. 8b and c, we can conclude that the porphine ring was easily polarized by the electrode comparing with saturated ring. For the Au–Por–Oc–Au, the relative electric charge of the porphine ring increases to 0.06 *e* from the value of 0.007 *e* for the saturated ring at 1.5 V. The asymmetric polarization under external electric field of Por–Oc is responsible for the nonlinear potential drop and further supports the asymmetric electron transport.

4. Conclusions

In summary, we found that constructing a barrier by placing a saturated ring between the molecule and the electrode greatly affects the electron transport in a metal–molecule–metal junction, since the electron transport is limited by the injection of charge carriers over the molecule–metal interfaces. Breaking electronic coupling is an efficient way of realizing rectification, though it may impede the current flow to a certain extent. Additionally, rectification is not only determined by the barrier height, but also sensitive to the barrier width. Although the same saturated ring is used in all models, a slight rectification is observed in linear and cyclic systems with low molecular proportion. The non-uniform potential drop induced by a tunneling barrier is responsible for the rectification. These results indicate that the coupling of organic molecules to metallic electrodes is required to be considered in the future design of molecular electronics.

Acknowledgements

Thanks to the National Natural Science Foundation of China (NSFC) (Funding Nos. 20821063 and 20873063), National Basic Research Program of China (973 Program, 2007CB936302) and the Open Project of State Key Laboratory of Applied Organic Chemistry (Lanzhou University) for financial support.

References

[1] A. Aviram and M. A. Ratner, *Chem. Phys. Lett*., 1974, **29**, 277.
[2] A. S. Martin, J. R. Sambles and G. J. Ashwell, *Phys. Rev. Lett*., 1993, **70**, 218.
[3] C. Joachim, J. K. Gimzewski and A. Aviram, *Nature*, 2000, **408**, 541.
[4] G. J. Ashwell, W. D. Tyrrell and A. J. Whittam, *J. Mater. Chem*., 2003, **13**, 2855.
[5] R. M. Metzger, *Chem. Rev*., 2003, **103**, 3803.
[6] K. Stokbro, J. Taylor and M. Brandbyge, *J. Am. Chem. Soc*., 2003, **125**, 3674.
[7] X. Yin, H. M. Liu and J. W. Zhao, *J. Chem. Phys*., 2006, **125**, 094711.
[8] H. M. Liu, P. Li, J. W. Zhao, X. Yin and H. L. Zhang, *J. Chem. Phys*., 2008, **129**, 224704.
[9] G. Leatherman, E. N. Durantini, D. Gust, T. A. Moore, A. L. Moore, S. Stone, Z. Zhou, P. Rez, Y. Z. Liu and S. M. Lindsay, *J. Phys. Chem. B*, 1999, **103**, 4006.
[10] V. B. Engelkes, J. M. Beebe and C. D. Frisbie, *J. Am. Chem. Soc*., 2004, **126**, 14287.
[11] J. Zhao, J. J. Davis, M. S. P. Sansom and A. Hung, *J. Am. Chem. Soc*., 2004, **126**, 5601.
[12] S. N. Yaliraki and M. A. Ratner, *J. Chem. Phys*., 1998, **109**, 5036.
[13] A. Danilov, S. Kubatkin, S. Kafanov, P. Hedegrd, N. Stuhr-Hansen, K. Moth-Poulsen and T. Bjrnholm, *Nano Lett*., 2008, **8**, 1.
[14] A. Grigoriev, J. Sko¨ ldberg, G. Wendin and Z˘ . Crljen, Phys. Rev. B: Condens. *Matter Mater. Phys*., 2006, **74**, 045401.
[15] Y. S. Park, A. C. Whalley, M. Kamenetska, M. L. Steigerwald, M. S. Hybertsen, C. Nuckolls and L. Venkataraman, *J. Am. Chem. Soc*., 2007, **129**, 15768.
[16] F. Chen, X. L. Li, J. Hihath, Z. F. Huang and N. J. Tao, *J. Am. Chem. Soc*., 2006, **128**, 15874.
[17] S. Martin, D. Z. Manrique, V. M. Garcia-Suarez, W. Haiss, S. J. Higgins, C. J. Lambert and R. J. Nichols, *Nanotechnology*, 2009, **20**, 125203.
[18] M. Kiguchi, T. Takahashi, M. Kanehara, T. Teranishi and K. Murakoshi, *J. Phys. Chem. C*, 2009, **113**, 9014.
[19] D. Walter, D. Neuhauser and R. Baer, *Chem. Phys*., 2004, **299**, 139.
[20] S. H. Ke, W. T. Yang and H. U. Baranger, *Nano Lett*., 2008, **8**, 3257.
[21] H. M. Liu, N. Wang, J. W. Zhao, Y. Guo, X. Yin, F. Y. C. Boey and H. Zhang, *ChemPhysChem*, 2008, **9**, 1416.
[22] J. A. Malen, P. Doak, K. Baheti, T. D. Tilley, R. A. Segalman and A. Majumdar, *Nano Lett*., 2009, **9**, 1164.
[23] N. Wang, H. Liu, J. Zhao, Y. Cui, Z. Xu, Y. Ye, M. Kiguchi and K. Murakoshi, *J. Phys. Chem. C*, 2009, **113**, 7416.
[24] H. Liu, W. Ni, J. Zhao, N. Wang, Y. Guo, T. Taketsugu, M. Kiguchi and K. Murakoshi, *J. Chem. Phys*., 2009, **130**, 244501.
[25] Z. Xu, N. Li, Y. P. Cui, H. M. Liu, H. B. Wang, Y. F. Ye and J. W. Zhao, *Chem. J. Chinese Univ*., 2009, **30**, 588.
[26] S. S. Mallajosyula and S. K. Pati, *J. Phys. Chem. B*, 2007, **111**, 11614.
[27] H. Basch, R. Cohen and M. A. Ratner, *Nano Lett*., 2005, **5**, 1668.
[28] Z. Y. Li and D. S. Kosov, *J. Phys. Chem. B*, 2006, **110**, 19116.
[29] J. Taylor, M. Brandbyge and K. Stokbro, *Phys. Rev. Lett*., 2002, **89**, 138301.
[30] S. Datta, *Electronic Transport in Mesoscopic Systems*, Cambridge University

Press, New York, 1997.
[31] F.-R. F. Fan, J. P. Yang, L. T. Cai, D. W. Price, S. M. Dirk, D. V. Kosynkin, Y. X. Yao, A. M. Rawlett, J. M. Tour and A. J. Bard, *J. Am. Chem. Soc.*, 2002, **124**, 5550.
[32] (a) Atomistix Toolkit version 2.0, QuantumWise A/S (www. quan tumwise. com); (b) J. M. Soler, E. Artacho, J. D. Gale, A. Garcia, J. Junquera, P. Ordejón and D. Sanchez-Portal, J. Phys.: Condens. Matter, 2002, 14, 2745; (c) J. Taylor, H. Guo and J. Wang, Phys. Rev. B: Condens. *Matter Mater. Phys*., 2001, **63**, 245407.
[33] See Atomistic Toolkit manual for details: http://www.quantum wise.com.
[34] M. J. Frisch, G. W. Trucks, H. B. Schlegel, G. E. Scuseria, M. A. Robb, J. R. Cheeseman, J. A. Montgomery, Jr., T. Vreven, K. N. Kudin, J. C. Burant, J. M.Millam, S. S. Iyengar, J. Tomasi, V. Barone, B. Mennucci, M. Cossi, G. Scalmani, N. Rega, G. A. Petersson, H. Nakatsuji, M. Hada, M. Ehara, K. Toyota, R. Fukuda, J. Hasegawa, M. Ishida, T. Nakajima, Y. Honda, O. Kitao, H. Nakai, M. Klene, X. Li, J. E. Knox, H. P. Hratchian, J. B. Cross, V. Bakken, C. Adamo, J. Jaramillo, R. Gomperts, R. E. Stratmann, O. Yazyev, A. J. Austin, R. Cammi, C. Pomelli, J. Ochterski, P. Y. Ayala, K. Morokuma, G. A. Voth, P. Salvador, J. J. Dannenberg, V. G. Zakrzewski, S. Dapprich, A. D. Daniels, M. C. Strain, O. Farkas, D. K. Malick, A. D. Rabuck, K. Raghavachari, J. B. Foresman, J. V. Ortiz, Q. Cui, A. G. Baboul, S. Clifford, J. Cioslowski, B. B. Stefanov, G. Liu, A. Liashenko, P. Piskorz, Komaromi, R. L. Martin, D. J. Fox, T. Keith, M. A. Al-Laham, C. Y. Peng, A. Nanayakkara, M. Challacombe, P. M. W. Gill, B. G. Johnson, W. Chen, M. W. Wong, C. Gonzalez and A. Pople, GAUSSIAN 03 (*Revision C.2*), Gaussian, Inc., Wallingford, CT, 2004.
[35] S. N. Yaliraki, A. E. Roitberg, C. Gonzalez, V. Mujica and M. A. Ratner, *J. Chem. Phys.*, 1999, 111, 6997.
[36] E. Livshits and R. Baer, *Phys. Chem. Chem. Phys*., 2007, **9**, 2932.
[37] S. J. A. van Gisbergen, J. M. Pacheco and E. J. Baerends, Phys. Rev. A: At., Mol., *Opt. Phys*., 2001, **63**, 063201.
[38] R. Baer and D. Neuhauser, *Phys. Rev. Lett*., 2005, **94**, 043002.
[39] R. Baer, E. Livshits and D. Neuhauser, *Chem. Phys*., 2006, **329**, 266.
[40] Z. Y. Li and D. S. Kosov, *J. Phys. Chem. B*, 2006, **110**, 9893.
[41] M. Brandbyge, J.-L. Mozos, P. Ordejón, J. Taylor and K. Stokbro, *Phys. Rev. B: Condens. Matter Mater. Phys*., 2002, **65**, 165401.
[42] G. Sedghi, K. Sawada, L. J. Esdaile, M. Hoffmann, H. L. Anderson, D. Bethell, W. Haiss, S. J. Higgins and R. J. Nichols, J. Am. Chem. Soc., 2008, 130, 8582.
[43] Z. Xu, N. Li, X. Jin, Y. Li, H. Liu and J. Zhao, *Chem. Lett*., 2007, **36**, 1278.
[44] J. G. Simmons, *J. Appl. Phys.*, 1963, **34**, 1793.

List of Figures

Scheme 1 (a) Schematic representation of the molecular junction. (b) The molecular structures of OPE system. L_c and L_s are the lengths of the conjugated and saturated parts, the molecular proportion is defined as $R = L_c/L_s$. For OPE–Oc, L_c = 16.68 Å , L_s = 2.61 Å , and R = 6.4. (c) The molecular structures of the porphine system: porphine (Por), porphine–benzene (Por–Ph) and porphine–octane (Por–Oc). For Por–Oc, L_c = 7.61 Å , L_s = 2.65 Å and R = 2.9

Figure. 1 The left panels show the calculated density of states (in arbitrary units) projected onto the molecular region (PDOS) of (a) OPE and (b) OPE–Oc. The right panels give the HOMO and LUMO spatial distribution of two models.

Figure. 2 (a) The potential drop along the OPE–Oc junction at 1.5 V. To evaluate the electric charge, we divided the OPE–Oc into 8 parts numbered below the image. (b) and (c) plot the electric charge per part relative to zero bias of free OPE–Oc and Au–OPE–Oc–Au junctions, respectively.

Figure. 3 (a) Representative semilog plot of the current–voltage (*I–V*) curves of OPE and OPE–Oc. The inset shows a linear plot of the *I–V* curve for OPE–Oc. (b) The rectification ratio of the linear system as a function of bias.

Figure. 4 Transmission spectra of (a) OPE and (b) OPE–Oc at typical bias. Fermi level of the electrode is set to zero in the transmission spectra. Molecular orbital energy levels near Au electrode Fermi level as a function of bias for (c) OPE and (d) OPE–Oc.

Figure. 5 (a) *I–V* curves obtained by NEGF formalism of the Por, Por–Ph and Por–Oc junctions and the inset is the *I–V* curve of Por–Oc. (b) Voltage dependence of the rectification ratio of three models.

Figure. 6 Transmission spectra of (a) Por, (b) Por–Ph, and (c) Por–Oc under various bias. The shadows denote the bias windows. Molecular orbital energy levels for the cyclic systems (d) Por, (e) Por–Ph, and (f) Por–Oc. The response of the molecular orbital energy levels to the applied bias is dependent on the molecules.

Figure. 7 (a) Left panel is the calculated PDOS of Por and the right panel shows the HOMO and LUMO spatial distribution of Por. (b) The center panel shows the PDOS of Por–Ph and Por–Oc. The left and right panels show the spatial distribution of Por–Ph and Por–Oc.

Figure. 8 (a) The potential drop of Por–Oc junction at 1.5 V. The Por–Oc molecule is divided into 4 parts. (b) and (c) plot the relative electric charge of per part of free Por–Oc and Au–Por–Oc–Au junction, respectively.

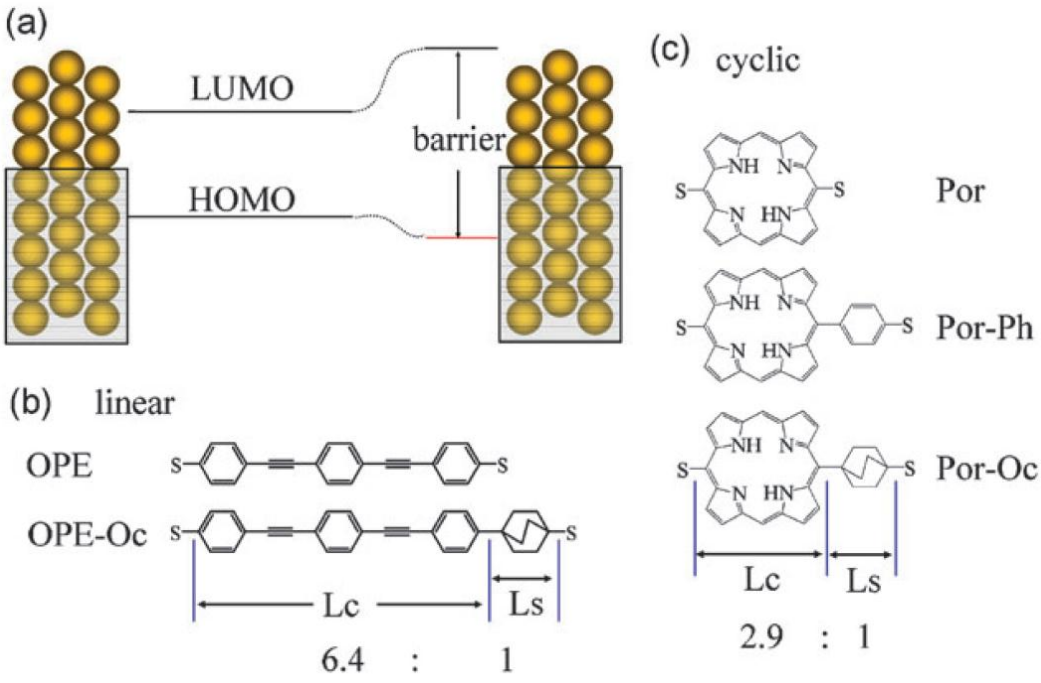
(a)
LUMO
barrier
HOMO
(b) linear
OPE
OPE-Oc
Lc
Ls
6.4 : 1
(c) cyclic
Por
Por-Ph
Por-Oc
Lc
Ls
2.9 : 1

Scheme 1

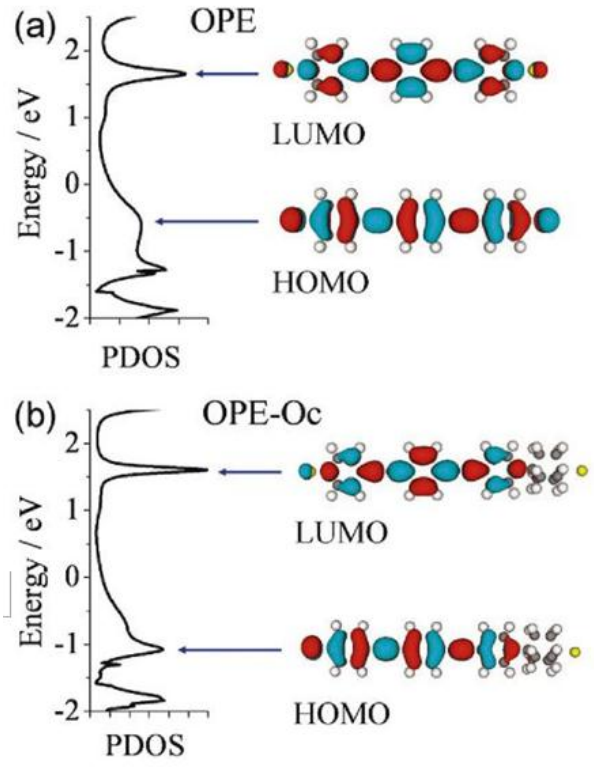
(a)
OPE
Energy / eV
2
1
0
-1
-2
PDOS
LUMO
HOMO
(b)
OPE-Oc
Energy / eV
2
1
0
-1
-2
PDOS
LUMO
HOMO

Figure 1

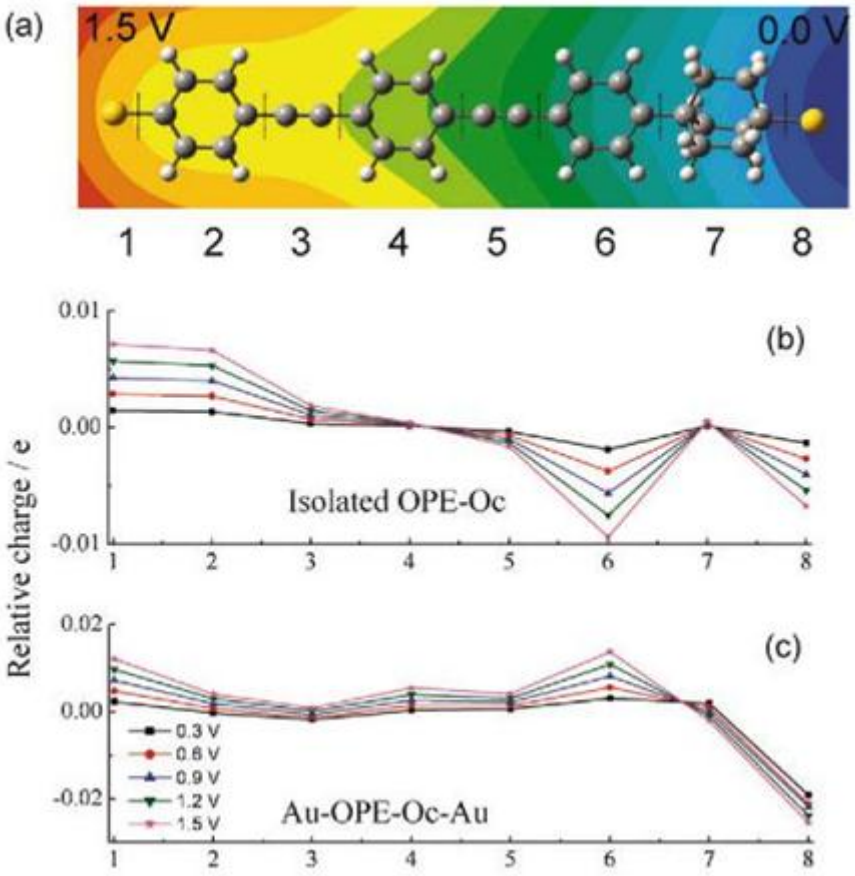
(a)
1.5 V
0.0 V
1 2 3 4 5 6 7 8
(b)
Isolated OPE-Oc
(c)
Au-OPE-Oc-Au
0.3 V
0.6 V
0.9 V
1.2 V
1.5 V
Relative charge / e
0.01
0.00
-0.01
0.02
0.00
-0.02

Figure 2

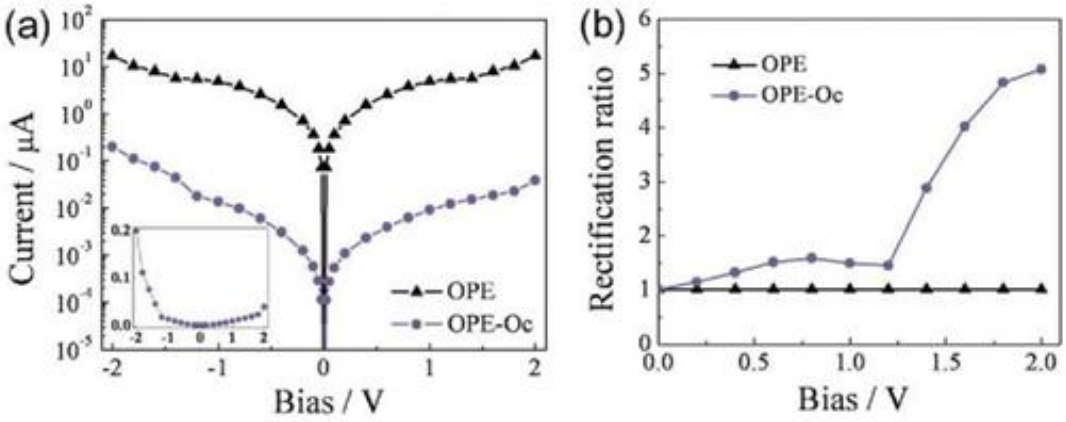
(a)
Current / μA
Bias / V
OPE
OPE-Oc
(b)
Rectification ratio
Bias / V
OPE
OPE-Oc

Figure 3

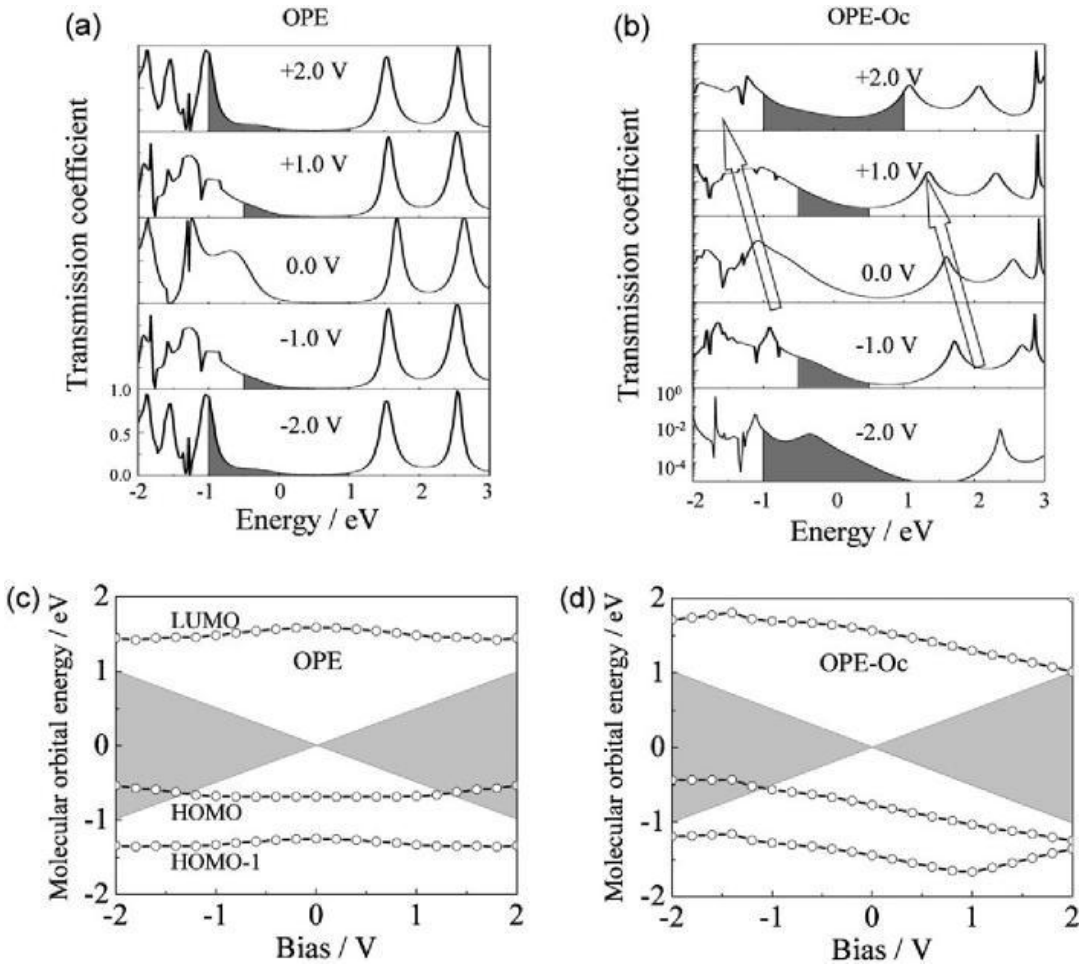
(a)
OPE
+2.0 V
+1.0 V
0.0 V
-1.0 V
-2.0 V
Transmission coefficient
Energy / eV
(b)
OPE-Oc
+2.0 V
+1.0 V
0.0 V
-1.0 V
-2.0 V
Transmission coefficient
Energy / eV
(c)
LUMO
OPE
HOMO
HOMO-1
Molecular orbital energy / eV
Bias / V
(d)
OPE-Oc
Molecular orbital energy / eV
Bias / V

Figure 4

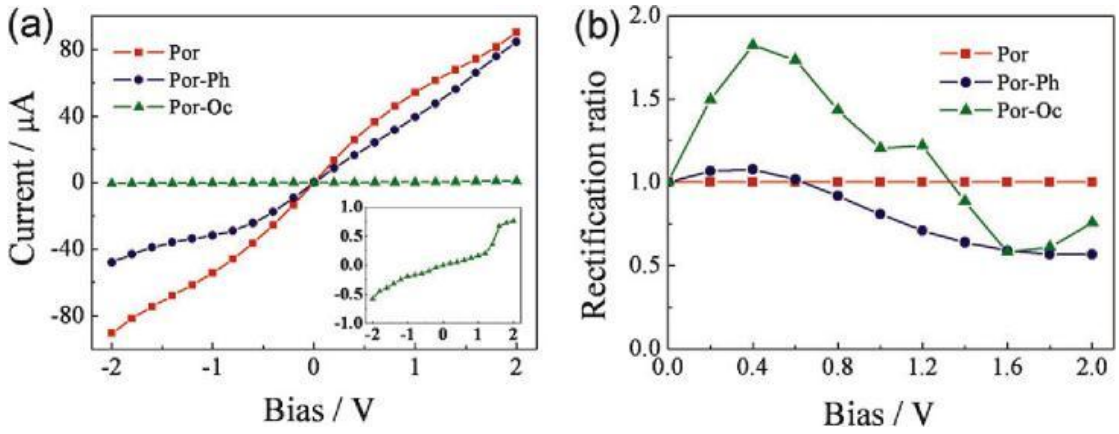
(a)
Por
Por-Ph
Por-Oc
Current / μA
Bias / V
(b)
Rectification ratio
Por
Por-Ph
Por-Oc
Bias / V

Figure 5

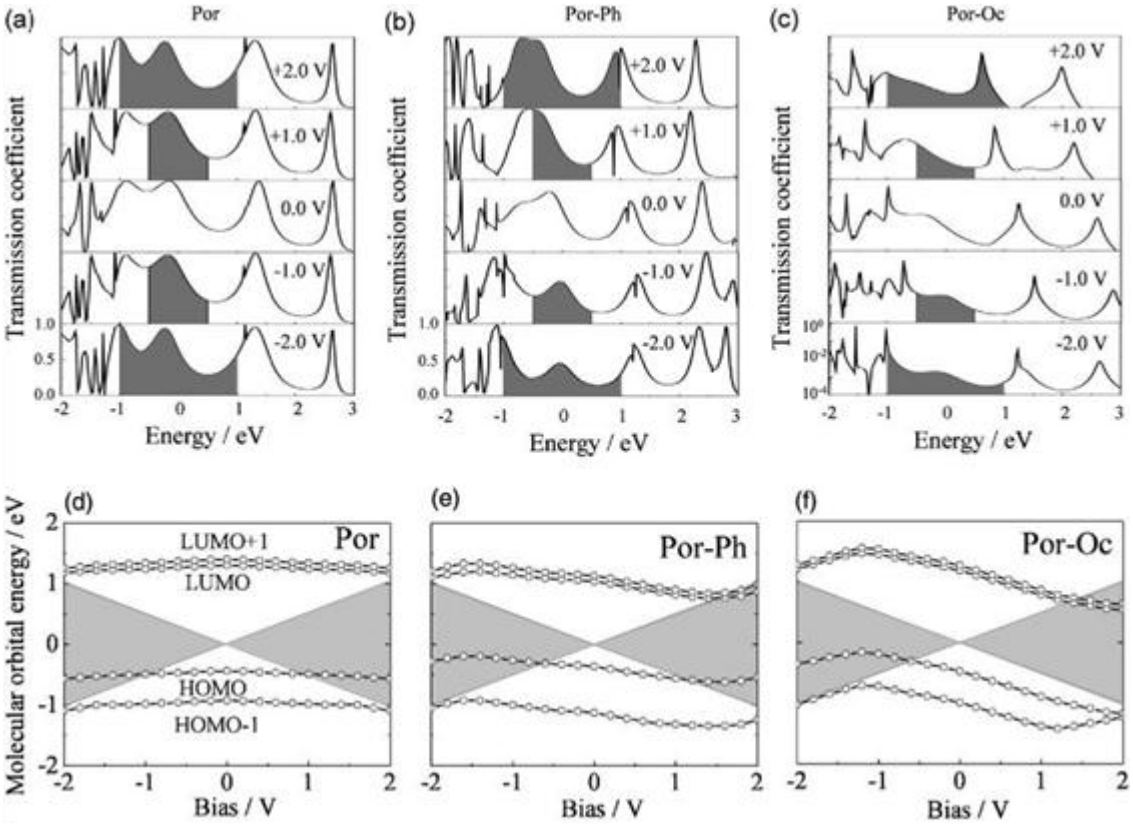
(a)
Por
(b)
Por-Ph
(c)
Por-Oc
Transmission coefficient
+2.0 V
+1.0 V
0.0 V
-1.0 V
-2.0 V
Energy / eV
(d)
(e)
(f)
Molecular orbital energy / eV
LUMO+1
LUMO
HOMO
HOMO-1
Bias / V

Figure 6

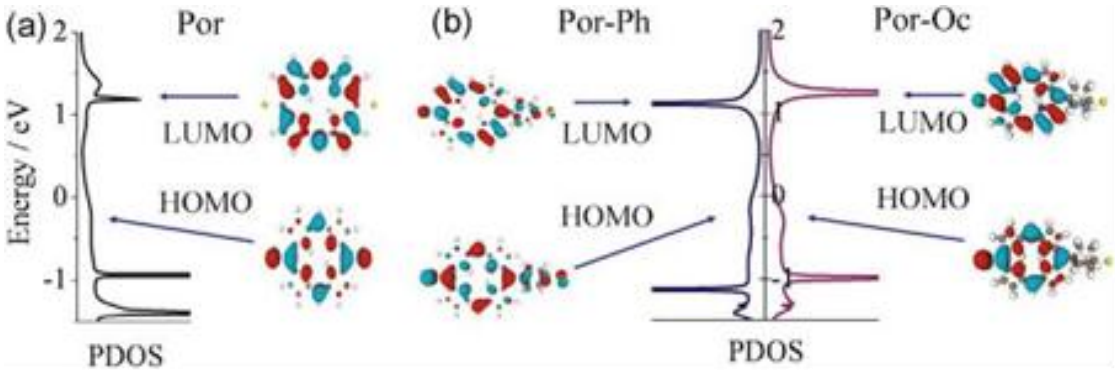
(a)
Por
2
1
0
-1
Energy / eV
LUMO
HOMO
PDOS
(b)
Por-Ph
Por-Oc
LUMO
HOMO
LUMO
HOMO
PDOS

Figure 7

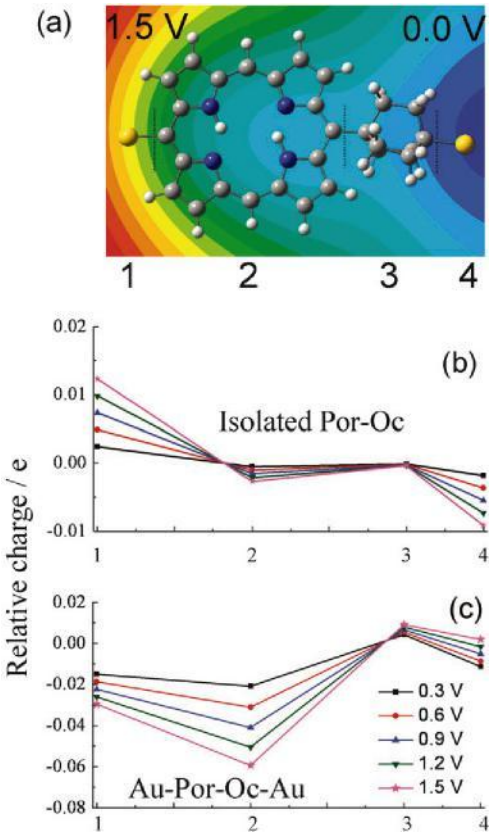
(a)
1.5 V
0.0 V
1
2
3
4
(b)
Isolated Por-Oc
(c)
Au-Por-Oc-Au
0.3 V
0.6 V
0.9 V
1.2 V
1.5 V
Relative charge / e
0.02
0.01
0.00
-0.01
-0.02
-0.04
-0.06
-0.08

Figure 8